Three-Dimensional Cubic Mesoporous Structures of SBA-12 and Related Materials by Electron Crystallography

Yasuhiro Sakamoto,[†] Isabel Díaz,[†,‡] Osamu Terasaki,*[,†,§] Dongyuan Zhao,[||,⊥] Joaquin Pérez-Pariente,[‡] Ji Man Kim,[||,#] and Galen D. Stucky[||]

Department of Physics, Tohoku University, Sendai 980-8578, Japan, Instituto de Catálisis y Petroleoquímica, CSIC, Campus Cantoblanco, 28049-Madrid, Spain, Center for Interdisciplinary Research, Tohoku University, Sendai 980-8578, Japan, Department of Chemistry & Biochemistry and Materials Department, University of California, Santa Barbara, California 93106, Department of Chemistry, Fudan University, Shanghai 200433, P. R. China, and Department of Molecular Science & Technology and Applied Chemistry, Ajou University, Suwon, 442-749, Korea

Received: November 8, 2001; In Final Form: January 23, 2002

The chemical potential difference between homopolymer fractions in block copolymers can be readily used to selectively design, and cooperatively assemble, inorganic species into highly ordered three-dimensional (3d) periodic composite arrays of separated mesoscale regions. The actual details and symmetry of these regions and their long-range order can only be determined by 3d imaging and analysis with high-resolution electron microscopy (HREM). Of particular interest is the differentiation between configurations with very similar organization energies, such as the cubic and hexagonal (SBA-2) closed-packed structures. Mesoporous silica SBA-12 and functionalized SBA-12 (SH−SBA-12) have been synthesized from the 3-mercaptopropyl group by using nonionic surfactant $C_{18}H_{37}(CH_2CH_2O)_{10}$ ($C_{18}EO_{10}$, Brij 76) under acidic hydrothermal condition. Relatively large single-phase domains were obtained in SH−SBA-12. The 3d structural solution of SH−SBA-12 was obtained by Fourier analyses of HREM images. The structure is composed of spherical cavities, which are arranged in a cubic close-packed structure, in which each cavity is connected to the twelve nearest-neighbor cavities through openings parallel to the ⟨110⟩ directions. HREM images of SBA-12 taken over large sample regions show that SBA-12 is a mixture of mostly the cubic close-packed phase, which consist of beautifully crystalline narrow bands with the same 3d structure in twin relation to each other and a relatively small amount of the 3d hexagonal close packed phase.

Introduction

A variety of silica mesoporous materials with different structures have been prepared by using the cooperative-organization of ionic surfactants and ionic silica species in water.[1−5] After the success of using nonionic surfactants for the synthesis of highly ordered mesostructures, a series of new 3d periodic mesoporous silicas (SBA series) with different structures were synthesized.[6,7]

These thick-walled, stable mesoporous materials have attracted a great deal of attention as molds in new materials syntheses,[8] catalysts,[9,10] low-dielectric coatings,[11] optical materials[12] and for other applications, as they are easily processible into a variety of morphologies, have pore diameters ranging from less than 1 nm[13] well into the mesopore range[6,7] and are structurally tunable.

Detailed structural information is valuable for their effective utilization and is hard to come by. Their structures have been initially characterized by powder X-ray diffraction (XRD) method. However, the powder XRD experiment is limited for structural studies of 3d-mesoporous silicas, because the large unit cells result in a small number of reflections in the XRD pattern which makes it difficult to unambiguously determine space groups and sometimes even their crystal systems. A much more powerful method for the structural determination of these systems is high-resolution electron microscopy (HREM). Recently by electron crystallography (EC), we showed that 3d-mesoporous structures could be solved uniquely,[13−15] and structure solutions for pure MCM-48,[13−16] SBA-1, SBA-6, and SBA-16[13] phases were reported. To apply this method for a 3d structural analysis, it is necessary to have a thin region of a certain volume (ca. 20 unit cells at least in lateral width) of one pure phase with good periodicity. However, only carefully prepared materials satisfy these conditions, so that it is not commonly easy to find such regions in 3d silica mesoporous materials.

SBA-2 was first reported as the product of a synthesis using charged gemini surfactants in 1995[5,17] and, based on powder X-ray and TEM data, proposed to be a 3d hexagonal cage structure with a space group (SG) $P6_3/mmc$. It was noted in this study that the lattice parameters obtained from the X-ray data were also consistent with a *hcp* structure. Later, more extensive TEM studies were carried out, and it was reported that SBA-2 is a mixture of a cubic and a hexagonal phase;[18] however, their structures were not solved. SBA-12 was subsequently synthesized using surfactant $C_{18}EO_{10}$ and based on X-ray diffraction and TEM evidence described as having the

* To whom correspondence should be addressed. E-mail: terasaki@msp.phys.tohoku.ac.jp.
[†] Department of Physics, Tohoku University.
[‡] Instituto de Catálisis y Petroleoquímica, CSIC.
[§] Center for Interdisciplinary Research, Tohoku University.
[||] University of California, Santa Barbara.
[⊥] Fudan University.
[#] Ajou University.

10.1021/jp014094q CCC: $22.00 © 2002 American Chemical Society
Published on Web 03/06/2002

3d hexagonal symmetry ($P6_3/mmc$) originally ascribed to SBA-2.[7] On the other hand, using $C_{16}EO_{10}$ as surfactant structure-directing agent, a cubic phase (assigned as SBA-11) with $m\bar{3}m$ point group was suggested. The data were not adequate to uniquely identify the space group for this cubic structure. On the basis of the results from these previous studies,[7,18] it was clear that at least two structural phases were in close proximity to each other in the synthesis phase space. It was also clear that a careful and more detailed 3d EC study of the silica phase produced with $C_{18}EO_{10}$ was needed. Preliminary 3d HREM studies at Tohoku University of a sample of the SBA-12 phase made at the University of California, Santa Barbara, showed intergrowth that was difficult to resolve. Synthesis and structural characterization of a functionalized phase synthesized with the same surfactant, $C_{18}EO_{10}$, in Madrid[19] was, however, more successful.

In this study, the 3d-cubic structure of the functionalized SBA-12 materials is determined by EC, even though it is not a single phase. Structural characterization of unfunctionalized SBA-12 is also described. The structural solution by EC of the 3d-hexagonal phases obtained from a different synthesis will be reported separately.

Intergrowth of Hexagonal and Cubic Phases and Twins in Cubic Phase. The most familiar problem of this type in zeolite systems, namely, the intergrowth of cubic FAU and hexagonal EMT, was carefully studied by both powder XRD and high-resolution electron microscope (HREM) images.[20] To make the problem for mesoporous materials easy to understand, consider the powder XRD patterns of cubic and hexagonal phases.[21] From elementary crystallography, the spacings of d_{hex} (hkl) for the hkl reflections in a hexagonal crystal with lattice constants a_{hex} and c_{hex} are given by the equation

$$(1/d_{hex}(hkl))^2 = 4(h^2 + hk + k^2)/3a_{hex}{}^2 + l^2/c_{hex}{}^2$$

whereas those for the cubic system with lattice constant a_{cub} are

$$(1/d_{cub}(hkl))^2 = (h^2 + k^2 + l^2)/a_{cub}{}^2$$

If we consider two hard sphere packed structures, that is, cubic close packed structure, *ccp*, (SG:$Fm\bar{3}m$) and hexagonal closed packed structure, *hcp*, (SG:$P6_3/mmc$), then

$$a_{cub} = \sqrt{2}a_{hex} \quad \text{and} \quad c_{hex}/a_{hex} = \sqrt{8/3} = 1.633.$$

Characteristic features of the peaks in powder XRD pattern for *hcp*, in the relatively low scattering angle region, are the appearances of 100_h, 002_h, and 101_h reflections together with 102_h, 110_h, 103_h, 200_h, and 112_h reflections. On the other hand, all of the reflections from the cubic phase overlap with those from the *hcp* phase, except the 200_c reflection, for example, peak positions for 111_c, 220_c, and 311_c reflections coincide with those for 002_h, 110_h, and 112_h, respectively. From this rule, by observing three reflections of 100_h, 002_h, and 101_h types, it is clear that the material is not cubic *F* type. However, we must be careful to evaluate the coexistence of *F*-; it is important to check the coexistence of F type if the material appears to be a pure 3d-hexagonal phase. In powder XRD experiments, preferred orientation effects make the situation more complex, and one must average out the preferred orientation in order to discuss structure models based on the relative intensity ratios of the observations.

It needs to be emphasized that in the case of FAU, SG is $Fd\bar{3}m$, so that the 200_c reflection is extinct for *Fd* or $F4_1$ types, but does appear in other *F* types. Thus, if the material is *Fd* or $F4_1$ type there is no reason to exclude the existence of a cubic phase. Conditions for the $00l$ reflections must be carefully checked in order to differentiate *Fd* or $F4_1$ types $\{00l:\ l = 4n\}$ from other *F* type $\{00l:\ l$ even$\}$ structures.

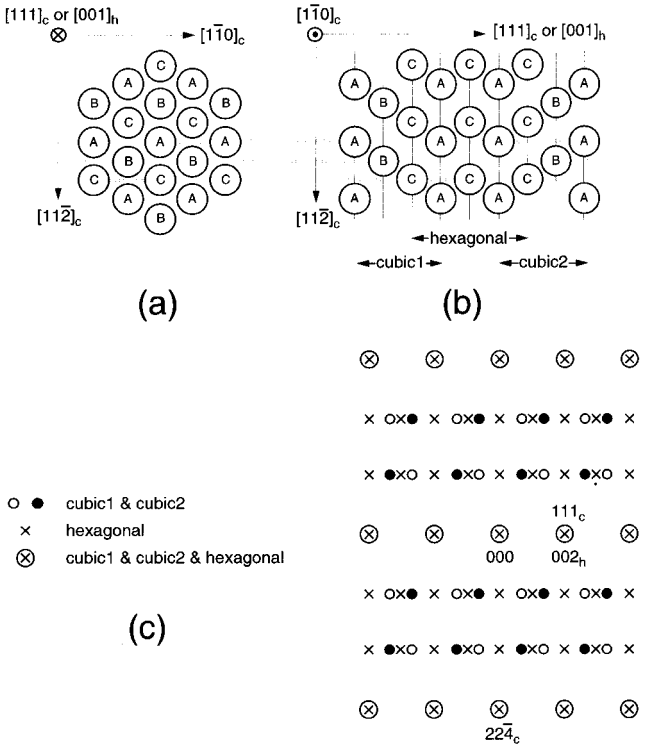

Figure 1. Schematic drawing of twins of ccp and hcp domain of 110 projection (a), and corresponding ED pattern (b).

Next, let us simply summarize twin structures, which are commonly observed in cubic *F* type system. Again taking the *ccp* of hard spheres ($Fm\bar{3}m$) as an example, the real and reciprocal spaces are schematically shown in Figure 1 parts a−c, respectively. A small *hcp* domain is also inserted for further discussion. In this case, the twin plane is $(111)_c$, and an average domain width of each twin is n times the $d(111)$ spacing. All diffraction spots will have streaks parallel to 111 with a length of $1/n$ times $1/d(111)$; therefore, if n is not too large, one can clearly see diffuse scattering.

Experimental Section

Sample Preparation. *Sample 1.* SBA-12: SBA-12 was synthesized using oligomeric alkyl-ethylene oxide surfactant Brij 76($C_{18}EO_{10}$) as described previously.[7] In a typical synthesis batch, 3.0 g of $C_{18}EO_{10}$ polymer were dissolved in 57.4 g of distilled water, and then 8.8 g of sodium metasilicate was added at room temperature with magnetic stirring, giving a clear solution. To this reaction mixture was quickly added 17.7 g of concentrated HCl with vigorous magnetic stirring. The resulting gel mixture was stirred for 1 day at room temperature and subsequently heated for 1 day at 373 K in an oven to increase the degree of silanol group condensation.

Sample 2. Functionalized SBA-12 (hereafter SH−SBA-12) gel containing the composition 0.95 TMOS:0.05 MPTS:2 HCl: 0.051 Brij 76:85 H_2O was prepared, where TMOS (tetramethoxysilane) and MPTS (3-mercaptopropyltrimethoxysilane). In a typical synthesis of thiol-containing SBA-12, Brij 76 was dissolved in acid solution (HCl 2N) and stirred for 30 min. Then, a mixture of TMOS and MPTS, previously stirred for 10 min, was added drop by drop. After aging the gel at

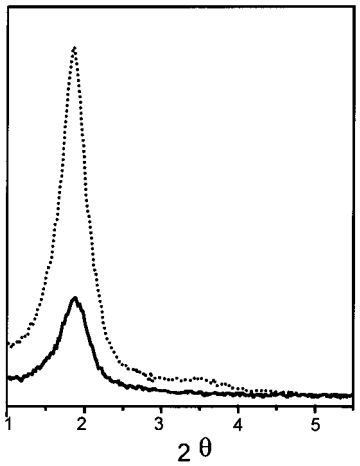

Figure 2. XRD of surfactant removed samples obtained from Brij 76, SBA-12/M (dot line) and thiol-containing SH−SBA-12 (solid line).

room temperature for 3h, the resulting filtered and washed thiol-containing solid was treated with ethanol at 343 K for 24 h in order to remove the surfactant and obtain the extracted sample, SH−SBA-12. For comparison proposes, the pure silica sample with the molar composition gel 1 TMOS:MPTS:2 HCl:0.051 Brij 76:85 H_2O was also prepared and is called SBA-12/M because the sample was synthesized in Madrid and the molar composition was in the ranges described by the report[7] and different from SBA-12.

The samples were characterized by Elemental Analyses, powder XRD experiment, HREM images, and nitrogen adsorption.

Sample Characterization. Analyses of the organic material present in the solids were done in a Perkin-Elmer 2400 CHN-analyzer (SH−SBA-12 extracted: 3.14% C, 1.44% H, 2.01% S). The incorporation of sulfur can be assessed by chemical analysis, which is 1.72 meq g^{-1}. The large amount of carbon present in the as-made material evidences the incorporation of the surfactant, which is quantitatively removed upon extraction, whereas the sulfur remains unaffected by this treatment and the C/S = 4.1.

X-ray powder diffraction patterns were collected using Cu Kα radiation, on a Seifert XRD 3000P diffractometer operating at low angle (2θ from 1 to 10°). The d spacing values of the thiol-containing sample are compatible with those reported for SBA-12, but the poorly resolved X-ray pattern avoids an unequivocal assignment of the symmetry (Figure 2).

Adsorption of nitrogen was carried out at 77 K in a Micromeritics ASAP 2000 apparatus. The nitrogen adsorption isotherm of extracted SH−SBA-12 was measured together with that of a pure-silica SBA-12 sample synthesized in the same conditions. The stepped nitrogen adsorption observed at p/p_0 values in the range 0.1−0.4 for the silica SBA-12/M shifts to lower pressure values for the thiol-containing SH−SBA-12. The incorporation of mercaptopropyl moieties reduces the mean pore diameter from 2.4 to 1.8 nm, and the surface area from 610 to 507 m^2 g^{-1}. The pore volume measured from nitrogen adsorption and calculated from the BJH method in the adsorption branch is 0.29 cm^3/g.

Electron Microscopy. For transmission electron microscopy (TEM), the samples were investigated with a JEM-3010, operating at 300 kV (Cs = 0.6 mm, resolution 1.7 Å). Images were recorded with films and a CCD-camera (model 794, Gatan, size 1024 × 1024, pixel size 25 × 25 μm) at 50 000−100 000 times magnification using low-dose conditions.

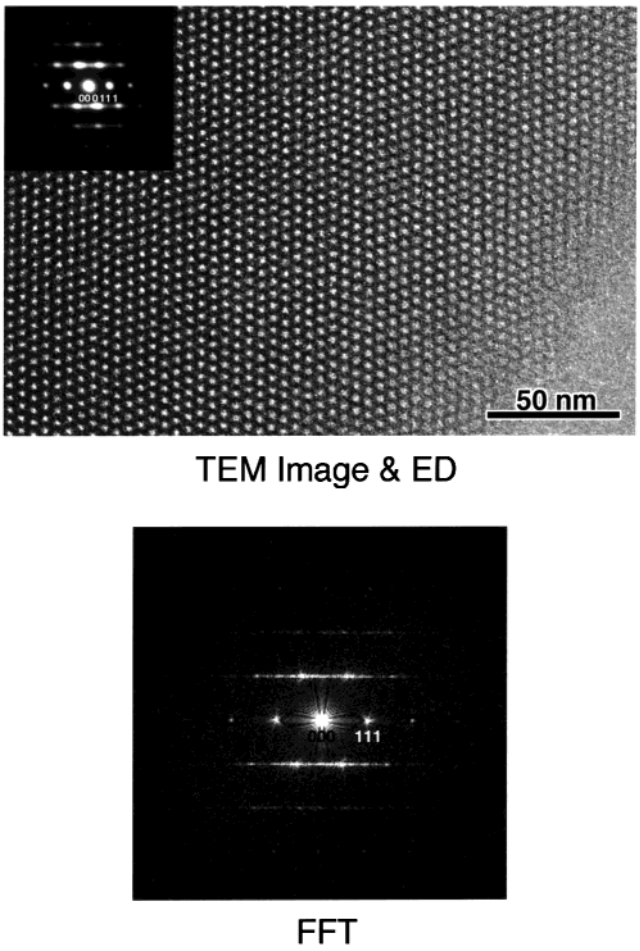

Figure 3. HREM image of SBA-12 and corresponding ED pattern (inset).

Image Processing. Fourier transforms were carried out using the images of thin parts of a crystal. They are complex in general, and their moduli as a function of wave vectors (in 2d k space) were displayed as Fourier diffractograms, from which extinction rules and hence the space group was determined. The transforms were corrected for the effect of the contrast transfer function (CTF) of the objective lens based on the weak phase object approximation as discussed previously.[13,14] Amplitudes and phases of diffraction peaks with a signal-to-noise ratio better than 3 were extracted from each Fourier transform. After confirming the space group symmetry, the symmetry of the space group was imposed on the amplitudes and phases. Phases were carefully extracted by extraction from several images, and amplitudes were determined from the highest-quality image for each incidence. Reflections, which are common for the different projections, were used to scale the amplitudes and to check that the same origin had been chosen in all projections. Inverse Fourier transforms of the obtained structure factors gave the 3d electrostatic potential map, that is, 3d structure of mesoporous crystal.

Results and Discussion

A typical HREM image observed from SBA-12 and a corresponding electron diffraction (ED) pattern (inset) is shown in Figure 3a, and Fourier diffractogram is shown in Figure 3b. The ED pattern clearly shows strong diffuse streaks along $[111]_c$. If the material is assumed to be cubic, which will be confirmed later, the direction of the incidence is $[1\bar{1}0]_c$. It is clear from the image that the crystal is composed of narrow cubic bands

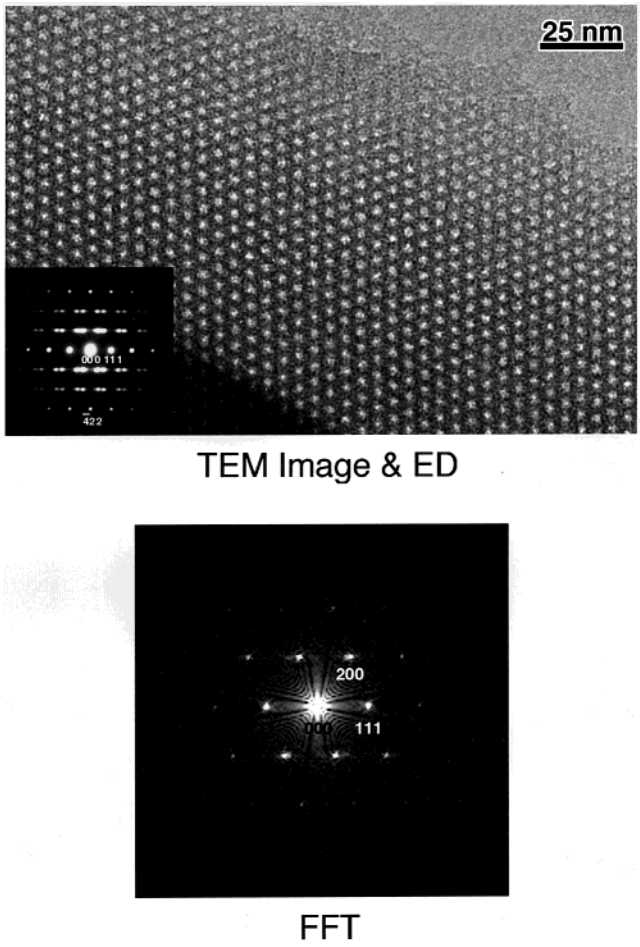

Figure 4. HREM image of SH−SBA-12 of [110] incidence and corresponding ED pattern (inset) (a) and Fourier diffractogram obtained from thin part of the image (b).

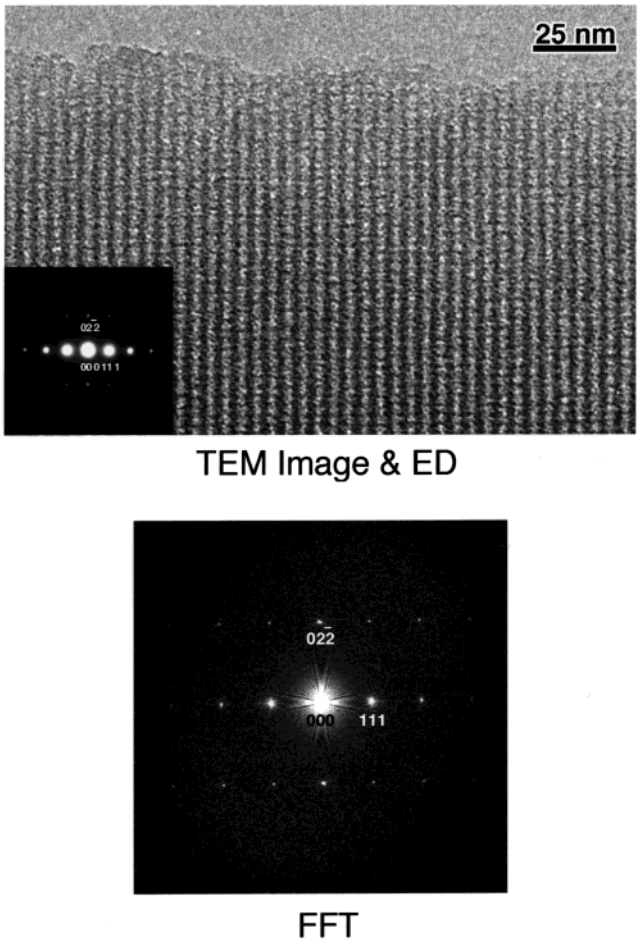

Figure 5. HREM image of SH−SBA-12 of [211] incidence and corresponding ED pattern (inset) (a) and Fourier diffractogram obtained from thin part of the image (b).

with beautiful periodicity in twin relation or an insertion of a thin slab of hexagonal and that the twin plane is $(111)_c$ running vertically. It was hard to obtain structural information from only one domain of SBA-12 by Fourier transform (FT) and also to take HREM images from other incident directions; therefore, the 3d-structure solution was not obtained by EC.

An HREM image observed from SH−SBA-12 is shown in Figure 4a together with the corresponding ED pattern. This phase was confirmed by both HREM images and ED patterns as cubic with lattice constant $a = 82$ Å, and the image (Figure 4) was taken with $[1\bar{1}0]$ incidence. As the size of the smallest selected area aperture is much larger than the area of Figure 4a, the inserted ED pattern is a superposition of that from twins. It is clear from the image that for this sample it is possible to find a large enough area to obtain structural information from one domain by FT. The Fourier diffractogram from a single domain is shown in Figure 4b as obtained from a thin area of Figure 4a. Structure factors of 111, 200, 220, 311, 222, 400, 331, 422, 511, and 333 reflections were obtained. From this Fourier diffractogram, it is clear, for example, that the appearance of the 200 reflection is not a multiple diffraction effect but is genuine; therefore, *Fd* or $F4_1$ types of structures should be discarded. The incident direction of this image is the same as that of Figure 3. Figure 5 shows another HREM image of SH−SBA-12 taken with [211] incidence from the same area of Figure 4 by tilting along the 111 axis, so that the strong 111 reflection is common for Figures 4 and 5. The FT of this image (Fourier diffractogram as shown in Figure 5 b) gives the structure factors of 111, 220, 311, 222, 420, 333, and 440 reflections. The conditions for observable reflections are summarized as {*hkl*: $h + k$, $k + l$, $l + h$ even}, {0*kl*: *k*,*l* even}, {*hhl*: $h + l$ even}, and {00*l*: *l* even}. Therefore $F\bar{4}3m$, *F*432, $Fm\bar{3}$, *F*23, and $Fm\bar{3}m$ are possible, and $Fm\bar{3}m$ was chosen as the highest space group.

TABLE 1: Crystal Structure Factors for Electrons of SH−SBA-12 Obtained by EC

hkl	*d* [Å]	F_{hkl}/F_{111}	phase
111	47.3	100.0	0
200	41.0	76.5	0
220	29.0	10.9	0
311	24.7	2.6	0
222	23.7	3.0	0
400	20.5	0.3	0
331	18.8	0.3	π
420	18.3	0.9	π

After correction of CTF and combining two different data sets through normalization by common reflections, a data set of 3d-crystal structure factors were determined as shown in Table 1, where relative factors are shown in the scale of $F_{111} = 100$, that is arbitrary. All of the structure factors up to the 420 reflection (spacings larger than 18.3 Å) are obtained. It should be mentioned here that *F*(*hkl*) is given by the product of the geometrical structure factor for *ccp* lattice, which is positive and equal to 4, and the FT of the pore structure. The negative sign of *F*(*hkl*) for 331 and 420 reflections might come from the sign of the FT of the pore structure at these wavenumbers. From the structure factors, the 3d-electrostatic potential (arbitrary

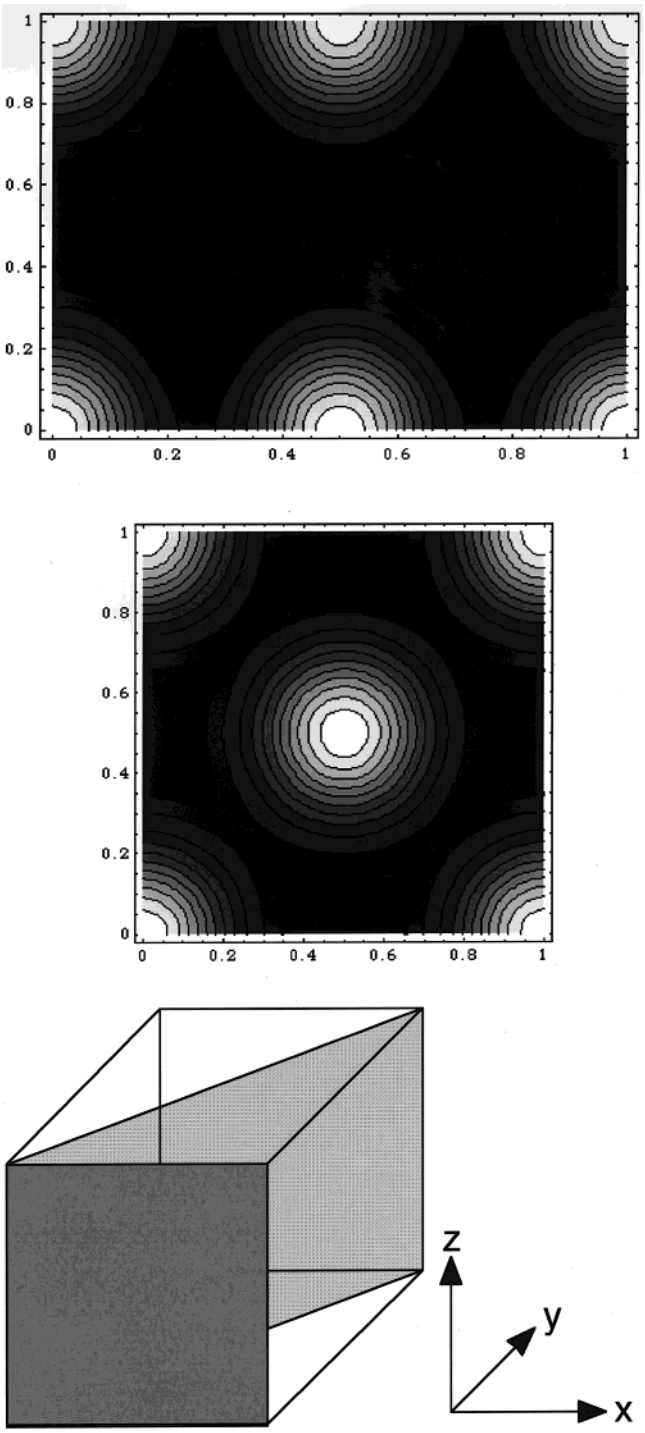

Figure 6. Electrostatic potential maps of SH−SBA-12. The sections at $y = 0$ (a) and $x = y$ (b) planes, the positions of which are schematically shown in c.

scale) map for electrons was uniquely obtained by calculating the inverse Fourier transform of the structure factors

$$f(x,y,z) = \sum_{h,k,l}[F(hkl)\cos 2\pi hx \cos 2\pi ky \cos 2\pi lz]$$

where $F(hkl)$ is the 3d-crystal structure factor for the hkl reflection shown in Table 1.

The map is shown in Figure 6 parts a and b, where equiconstant potential curves ($f(x,y,z) =$ constant) were drawn for the $y = 0$ and $x = y$ planes (Figure 6c), respectively. This solution is more realistic than the solid display as shown in the previous papers,[13,14] as this description gives the degree of local fluctuation of the surface by the slope in an average potential. Figure 7 shows a relation between the volume-fraction of pores and the value of constant ($f(x,y,z) =$ constant) in the potential density map. If it were possible to obtain a pure single phase, then by obtaining the pore volume from other experiments, such as gas adsorption isotherms, it would be possible to determine the constant necessary to more accurately define the boundary between pore and wall.

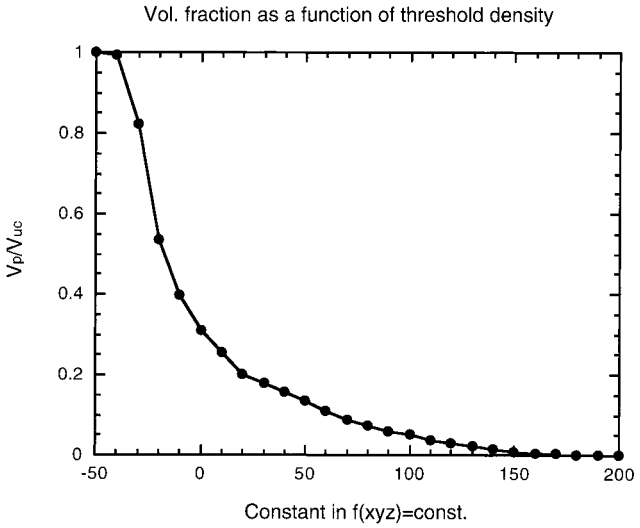

Figure 7. Relation between the volume fraction of the pores in the electrostatic potential density map.

When $f(x,y,z) = -20$, the spherical pores just contact each other and the pore volume fraction is 0.536. Therefore, if the volume fraction of pores is larger than this critical value, 0.536, all of the pores are connected each other. If we assume the average density of the pore wall of SH−SBA-12 as being 2.2 g cm^{-3}, the pore volume should be larger than 0.525 cm^3/g in order to include pore interconnections large enough to allow the washing out of the surfactant by ethanol. However, the observed pore volume is 0.29 cm^3/g. This fact points to a severe restriction of the accessibility of the large cavities to the N_2 molecules at the liquid nitrogen temperature. In regard to this, the *t* plot shows the presence of micropores with a surface area of 160 m^2/g, being the total area of the sample 507 m^2/g. Further evidence of sterical constraints for diffusion is given by the catalytic activity of SH−SBA-12 in the esterification of glycerol with oleic acid.[19] The turnover for this reaction is only $^1/_3$ of the functionalized MCM-41. Furthermore, the influence of the cubic/hexagonal intergrowth on the accessibility to the large spherical cavities remains to be studied yet.

The 3d-structure of SBA-12 corresponding to $f(x,y,z) = -25$ is shown in Figure 8 in order to show the 3d structure of the pores and their arrangement.

In the images, we could find small domains of the 3d-hexagonal structure, but they were too small for EC structural analysis. A large area of 3d hexagonal $P6_3/mmc$ was obtained in a different system, and its structure solution by EC will be discussed separately together with its structural relationship to the $Fm\bar{3}m$ structure described in this manuscript.

Summary

The similar organization energies of the *hcp* and *ccp* lattices found for crystalline and hard sphere packing clearly also exists for the amorphous silica wall structures formed with block polymer surfactants. The *ccp* arrangement of spherical cavities

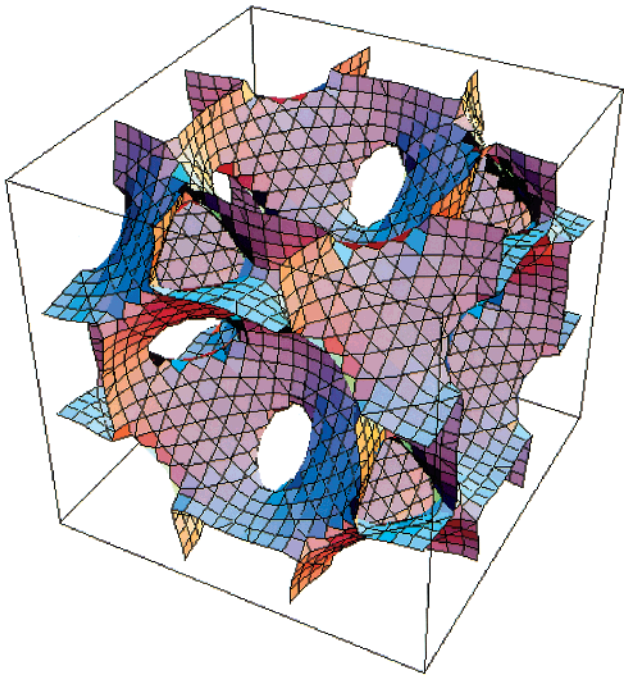

Figure 8. Mathematical drawing of 3d arrangement of pores for one of the fraction, $f(x,y,z) = -25$.

is found in SBA-12, with each cavity connected to its twelve nearest-neighbor cavities through openings parallel to the ⟨110⟩ directions. HREM images of SBA-12 taken over large sample regions show that SBA-12 is a mixture of mostly the cubic close-packed phase, which consist of highly crystalline narrow bands with the same 3d-structure in twin relation to each other, and a relatively small amount of the 3d hexagonal close packed phase. The variations obtained by different synthesis procedures suggests that the nature of the intergrowth in ordered mesostrucured phases is tunable, a matter of some interest in the hierarchical ordering of the pores of these structures for low dielectric and catalytic applications.[22]

Acknowledgment. A part of this study was supported by CREST program, Japan Science and Technology Corporation (O.T.). A fellowship from JSPS for Y.S. and a travel grant from the Spanish Ministry of Education for I.D. are acknowledged. Funding from the NSF of China (D.Y.Z.), United States National Science Foundation (G.D.S. and J.M.K.) also supported this research.

References and Notes

(1) Kresge, C. T.; Leonowicz, M. E.; Roth, W. J.; Vartuli, J. C.; Beck, J. S. Ordered mesoporous molecular-sieves synthesized by a liquid-crystal template mechanism. *Nature* **1992**, *359*, 710.

(2) Beck, J. S.; Vartuli, J. C.; Roth, W. J.; Leonowicz, M. E.; Kresge, C. T.; Schmitt, K. D.; Chu, C. T. W.; Olson, D. H.; Sheppard, E. W.; McCullen, S. B.; Higgins, J. B.; Schlenker, J. L. A new family of mesoporous molecular-sieves prepared with liquid-crystal templates. *J. Am. Chem. Soc* **1992**, *114*, 10834.

(3) Huo, Q.; Margolese, D. I.; Ciesla, U.; Feng, P. Y.; Gier, T. E.; Sieger, P.; Leon, R.; Petroff, P. M.; Schüth, F.; Stucky, G. D. Generalized synthesis of periodic surfactant/inorganic composite materials. *Nature* **1994**, *368*, 317.

(4) Huo, Q. S.; Margolese, D. I.; Ciesla, U.; Demuth, D. G.; Feng, P. Y.; Gier, T. E.; Sieger, P.; Firouzi, A.; Chmelka, B. F.; Schüth, F.; Stucky, G. D. Organization of organic molecules with inorganic molecular species into nanocomposite biphase arrays. *Chem. Mater.* **1994**, *6*, 1176.

(5) Huo, Q.; Leon, R.; Petroff, P. M.; Stucky, G. D. Mesostructure design with gemini surfactants—supercage formation in a 3-dimensional hexagonal array. *Science* **1995**, *268*, 1324.

(6) Zhao, D.; Feng, J.; Huo, Q.; Melosh, N.; Fredrickson, G. H.; Chmelka, B. F.; Stucky, G. D. Triblock copolymer syntheses of mesoporous silica with periodic 50 to 300 Angstrom pores. *Science* **1998**, *279*, 548.

(7) Zhao, D.; Hou, Q.; Feng, J.; Chmelka, B. F.; Stucky, G. D. Nonionic triblock and starblock surfactant syntheses of highly ordered, hydrothermally stable, mesoporous silica structures. *J. Am. Chem. Soc* **1998**, *120*, 6024.

(8) Jun, S.; Joo, S. H.; Ryoo, R.; Kruk, M.; Jaroniec, M.; Liu, Z.; Ohsuna. T.; Terasaki, O. Synthesis of New Nanoporous Carbon with Hexagonally Ordered Mesostructure. *J. Am. Chem. Soc.* **2000**, *122*, 10712.

(9) Yiu, H. H. P.; Wright, P. A.; Botting, N. P. Enzyme immobilization using SBA-15 mesoporous molecular sieves with functionalized surfaces. *J. Mol. Catal. B: Enzymol.* **2001**, *15*, 81.

(10) Yue, Y. H.; Gedeon, A.; Bonardet, J. L.; d'Espinose, J. B.; Melosh, N.; Fraissard, J. Direct incorporation of Al in SBA mesoporous materials: Characterization, stability and catalytic activity. *Stud. Surf. Sci. Catal.* **2000**, *129*, 209.

(11) Zhao, D.; Yang, P.; Melosh, N.; Feng, J.; Chmelka, B. F.; Stucky, G. D. Continuous mesoporous silica films with highly ordered large-pore structures. *Adv. Mater.* **1998**, *10*, 1380.

(12) Yang, P.; Wirnsberger, G.; Huang, H. C.; Cordero, S. R.; McGehee, M. D.; Scott, B.; Deng, T.; Whitesides, G. M.; Chmelka, B. F.; Buratto, S. K.; Stucky, G. D. Mirrorless lasing from mesostructured waveguides patterned by soft lithography. *Science* **2000**, *287*, 465.

(13) Sakamoto, Y.; Kaneda, M.; Terasaki, O.; Zhao, D.; Kim, J.-M.; Stucky, G. D.; Shin, H. J.; Ryoo, R. Direct imaging of the 3D pores and cages of mesoporous materials. *Nature* **2000**, *408*, 449.

(14) Carlsson, A.; Kaneda, M.; Sakamoto, Y.; Terasaki, O.; Ryoo, R.; Joo, S. H. The structure of MCM-48 determined by electron crystallography. *J. Electron Microsc.* **1999**, *48*, 795.

(15) Thomas, J. M.; Terasaki, O.; Gai, P. L.; Zhou, W.; Gonzalez-Calbet, J. Structural Elucidation of Microporous and Mesoporous Catalysts and Molecular Sieve. *Acc. Chem. Res.* **2001**, *34*, 583.

(16) Kaneda, M.; Tsubakiyama, T.; Carlsson, A.; Sakamoto, Y.; Ohsuna, T.; Terasaki, O.; Joo, S. H.; Ryoo, R. Structural Study of Mesoporous MCM-48 and Carbon Networks Synthesized in the Spaces of MCM-48 by Electron Crystallography. *J. Phys. Chem. B* in press 2002.

(17) Huo, Q. S.; Margolese, D. I.; Stucky, G. D. Surfactant control of phases in the synthesis of mesoporous silica-based materials. *Chem. Mater.* **1996**, *8*, 1147.

(18) Zhou, W.; Hunter, H. M. A.; Wright, P. A.; Ge, Q.; Thomas, J. M. Imaging the Pore Structure and Polytypic Intergrowths in Mesoporous Silica. *J. Phys. Chem. B* **1998**, *102*, 6933.

(19) Díaz, I.; Mohino, F.; Pérez-Pariente, J.; Sastre, E. Synthesis and Catalytic Properties of SO_3H-Mesoporous Materials from Gels Containing Non-Ionic Surfactants. *Stud. Surf. Sci. Catal.* **2001**, *135*, 1383.

(20) Ohsuna, T.; Terasaki, O.; Carr, S. W.; Anderson, M.; Alfredsson, V.; Bovin, J.-O.; Watanabe, D. Observations on the role of crownether templates in the formation of hexagonal and cubic polymorphs of zeolite Y. *Proc. R. Soc. London* **1996**, *452*, 715.

(21) Suffixes of hex or cub are indicated to distinguish two crystal systems, if necessary, otherwise all indices will be based on the cubic system.

(22) Bedard, R. L. Functional materials design for the new millennium: updating the rational strategy and enabling tools. *AIChE J.* **1999**, *45*, 2472.